Chapter 4

Optical modeling and measurement

In this chapter, modeling of the optical system is presented. The quality of the fabricated 45 °mirror, including its reflectivity and the deterioration of the incident beam are discussed.

4.1 Pickup optical system

The main components of the proposed planar integrated pickup are a long working distance fiberlens, a 45 °reflective mirror and a hemispherical SIL. In this case, light is guided by the core of the fiber and focused by the long-working-distance fiberlens on the bottom of the solid immersion lens. The Zemax modeling is shown in Fig. 4-1. The distance between the SMF and the microlens is filled with a pure silica rod of the same diameter and the same refractive index as the core of the SMF to avoid reflection. Meanwhile, only the case where the center of the incident mode field coincides with the optical axis is treated and the wave front of the incident beam from the core is planar. Only on-axis aberrations such as spherical aberration is considered in the analysis. The length of the pure silica rod g is used to control the focused beam size and its focal position. The parameters shown in Fig. 4-1 are designed for the fabrication geometry of the pickup, a fiber collimator with specific dimension is shown in Fig. 4-1 (a) and a weak focusing lens is shown in Fig. 4-1 (b), respectively. The effective numerical aperture (NA_{eff}) and Seidel coefficient (W_{040}) as a function of propagation distance g are shown in Fig. 4-2. Both increase with increased length of

silica rod g. In the case of g = 0.2 mm, the incident beam is almost collimated by the fiberlens at the cost of NA_{eff} reduction. In the other extreme case of g = 0.6 mm, the NA_{eff} can achieve 0.7 at the expanse of a short working distance and tight tolerance of the fabrication process.

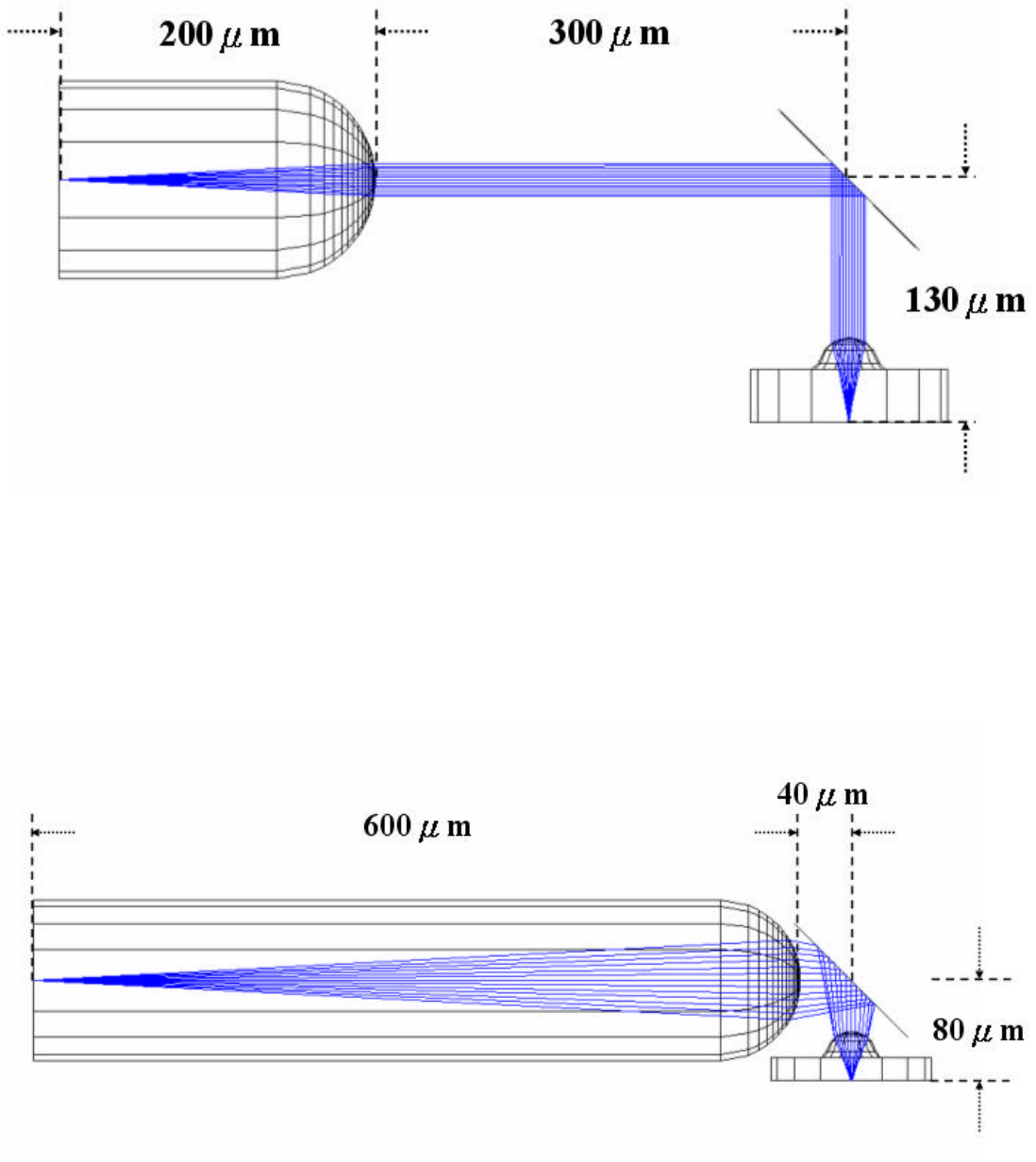

Fig. 4-1 (a) The fiberlens is used as a collimator, and (b) as a weak focusing lens

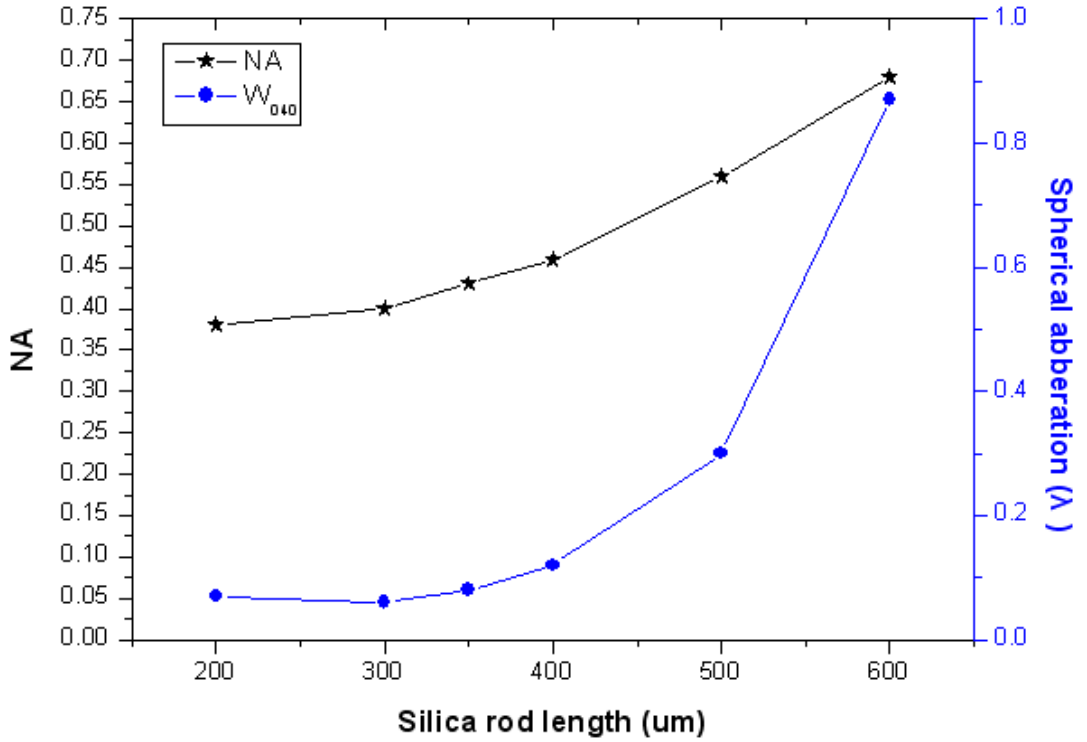

Fig. 4-2 The relationships of effective numerical aperture (NA_{eff}) and Seidel coefficient (W_{040}) as a function of propagation distance g

For our applications, a hemispherical-shaped fiberlens with radius = 62.5 μm and silica rod length g = 200 μm was chosen. There are two reasons: (1) the gap d between the fiberlens and the 45° mirror is difficult to control since the precision of fiber fixing machine is only 1mm. Therefore, a fiber collimator with g = 200 μm was used. The schematic is shown in Fig. 4-3.

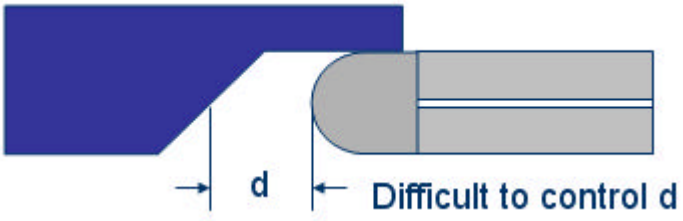

Fig. 4-3 The difficulty of controlling the gap d

(2) the aperture was realized by electroplating with a dimension of about 400 nm and 1 μm in thickness. Some light will be obstructed by the edge of the aperture if a high NA objective lens is applied, as shown in Fig. 4-4. To avoid such an ill effect, a small NA objective lens should be used. Therefore, a fiber collimator with g = 200 μm was chosen.

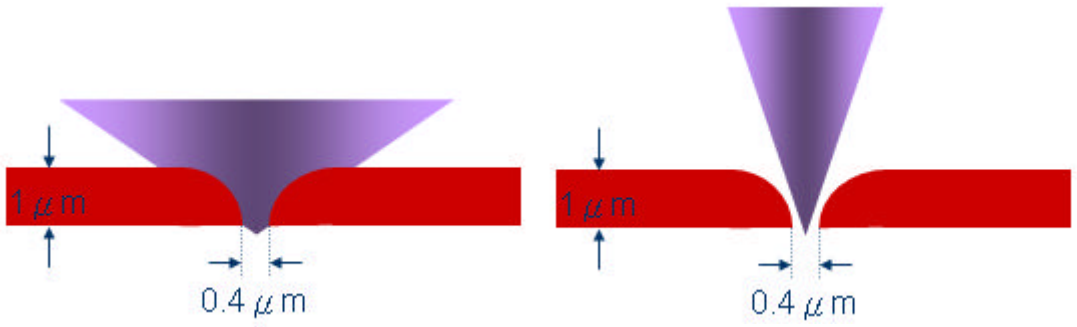

(a) (b)

Fig. 4-4 The phenomenon of (a) high NA and (b) small NA objective lens

4.2 Pickup optical throughput

The aperture here is used to further reduce the spot size of the overall system. An optical system that combines the microlens/aperture with fiber illumination exhibits several advantages. The spot size is mainly determined by the aperture size. Moreover, the optical throughput can be improved by several orders of magnitude over the aperture alone with either fiber-based or far-field illumination. In order to produce the possibly smallest spot with adequately large throughput, the aperture size cannot be reduced without any limitation. Therefore, there is a trade-off between the aperture size and the optical throughput. As shown in Fig. 4-5, the optical throughput, defined by the ratio of light power through the aperture to the fiber illumination is from 60% to 0% while the aperture radius ranging from about 1000 nm to 10 nm, respectively.

The dependence of the throughput on aperture size, effective numerical aperture (NA_{eff}) and Seidel coefficient (W_{040}) can be evaluated by Diffract.

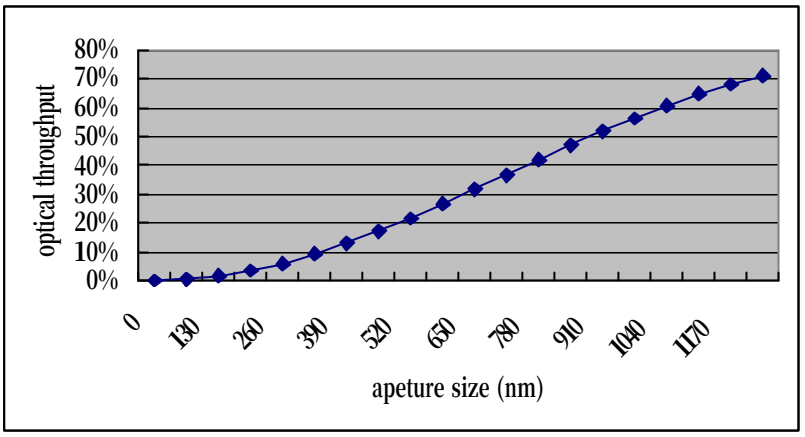

Fig. 4-5 The optical throughput decreases with increasing aperture radius

4.3 Optical measurement system

The measurement setup consists of a laser source, an attenuator, a 45 °reflective mirror, a two-axis (x-y) fiber coupler, a two-axis (x-z) stage, and an image CCD, as shown in Fig. 4.6. The spot diagram and the energy distribution can be measured and analyzed by the computer. All the measurement components except the laser and the attenuator were fixed on an optical rail to maintain the alignment along the optical axis. The intensity of the laser source is 20mW. The wavelength is 632.8 nm. The surface roughness of 45 °reflective mirror fixed on the optical rail is 25 nm in RMS value, 3 cm in radius, and 10 m in curvature. The SMF is 125 μm in diameter, 5 μm in core diameter. The hemispherical microlens fabricated on the front-end of the fiber, which is 62.5 μm in radius and has the same refractive index as the core of the SMF. A 10 X lens was mounted on the CCD to compensate for the large pixel size (3 μm × 4 μm) relative to the spot size out of the fiber (~ 10 μm).

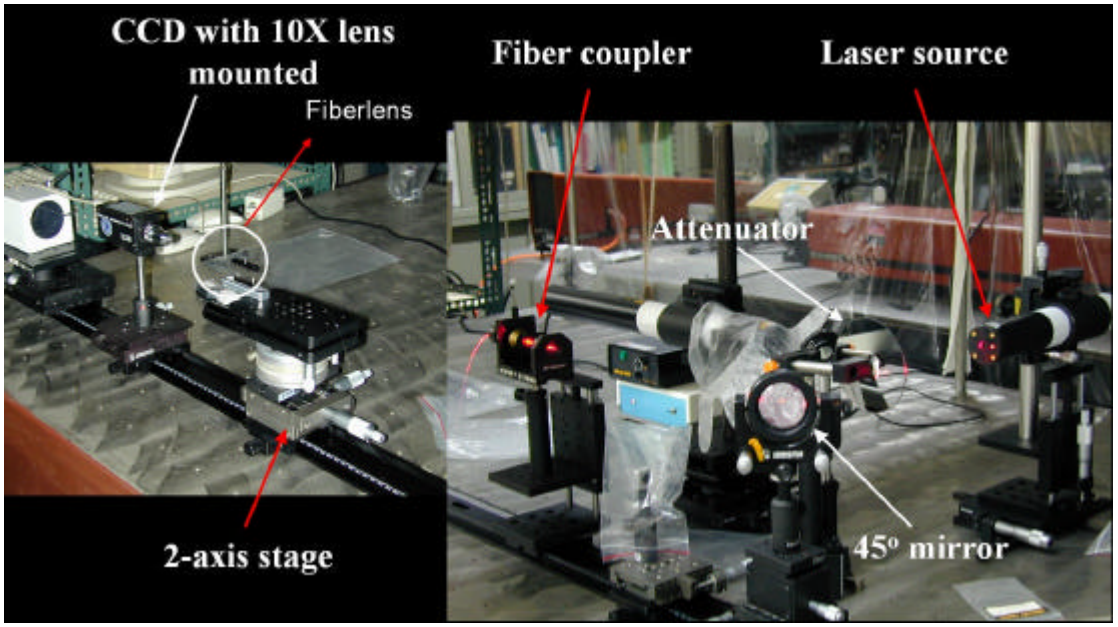

Fig. 4.6 The measurement system of the fiberlens/V-groove combination

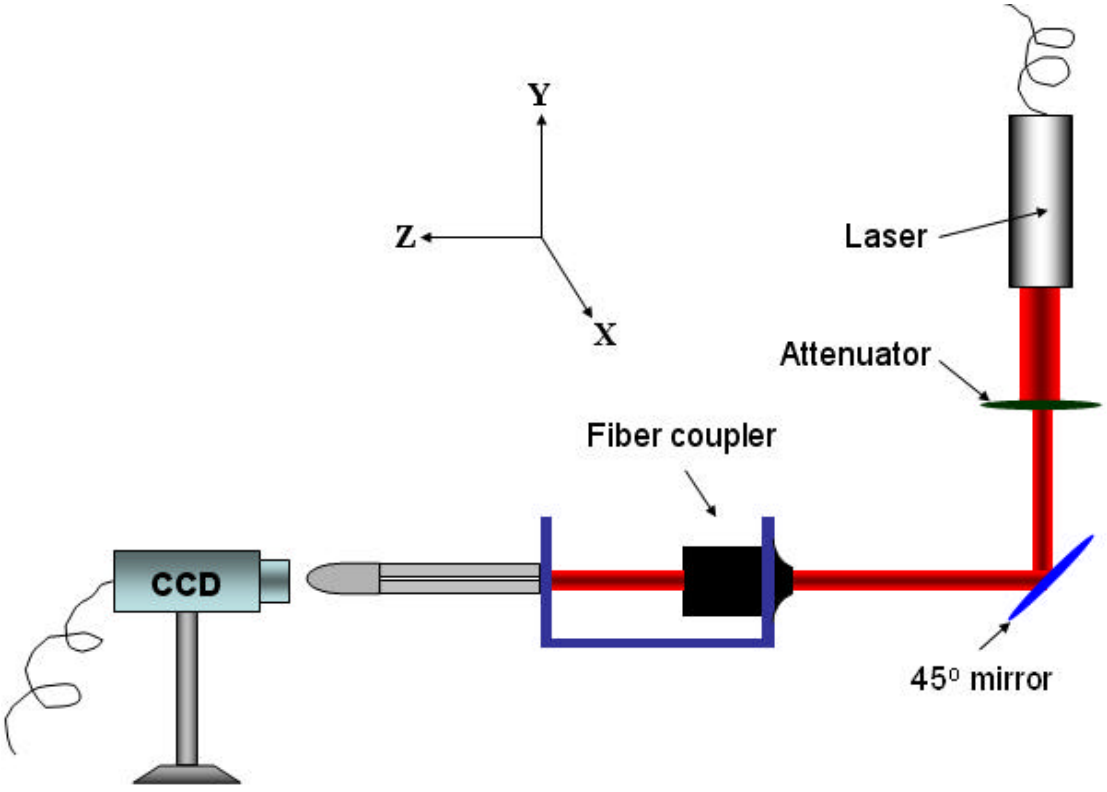

Fig. 4-7 A schematic view of the measurement system

The schematic of the measurement system is shown in Fig. 4-7. The intensity of laser source is reduced to a permissible degree by the attenuator so that it can be received by the CCD. The light is reflected by a 45 °mirror, and coupled into the fiber. The front end of the fiber was fixed on a two-axis (x-z) stage so the position of the spot and the distance between the fiberlens and the CCD can be adjusted by the stage. Finally, the light is received and analyzed by the CCD and the computer, respectively.

By using this measurement setup, the spot size, spot diagram, energy distribution, beam shape, and divergent angle out of the fiberlens can be measured and determined. Furthermore, the reflectivity of the fabricated V-groove together with 45 °mirror can be also determined by comparing the measured intensity with the 45 °mirror added or not.

4.4 Fiberlens measurement

4.4.1 Mathematical description

We designed a fiberlens with a large radius **R** compared to other published works [37-38]. The distance between the SMF and the microlens is filled with a pure silica rod of the same diameter and same refractive index as the core of the SMF to avoid reflection, as shown in Fig. 4-8. The mode field radius W_0 is computed by the following formula[39].

$$\frac{W_0}{a} = 0.65 + \frac{1.619}{V^{3/2}} + \frac{2.879}{V^6} \qquad (4\text{-}1)$$

where a is the core radius of the step-index fiber and V is the normalized frequency $V = \frac{2\pi}{\lambda} a\sqrt{n_1^2 - n_2^2}$ (n_1 and n_2, are the refractive indices of the core and cladding, respectively). The mode field diameter $2W_0$ at wavelength λ = 0.63 μm is about 4.3 μm.

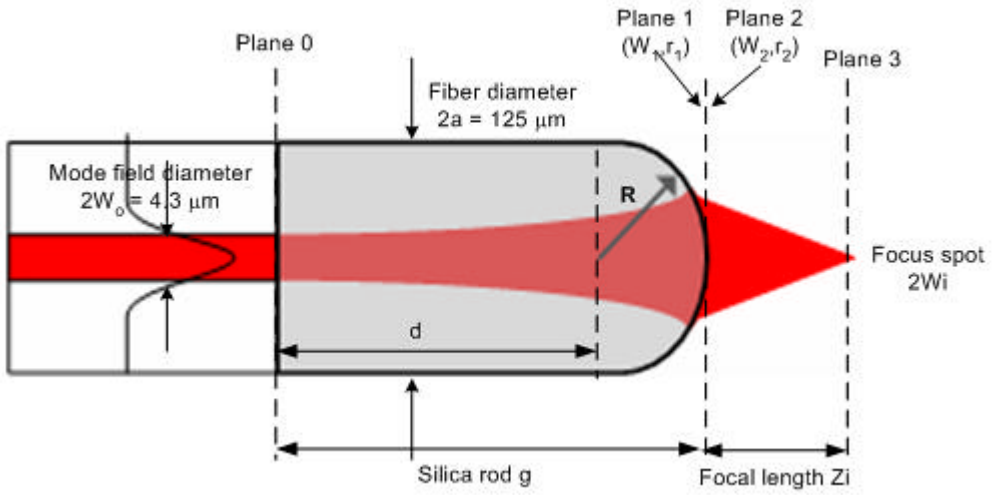

Fig. 4-8 Illustrated schematics of the microlens on the end face of the SMF (refractive index of the silica rod n = 1.45, cladding diameter 2a = 125 μm, mode field diameter $2W_0$ = 4.3 μm at λ = 0.63 μm)

By applying the ABCD law to the thick microlens system, W_1 and r_1, beam waist and radius at output plane RP_{OUT} (Plane 1) can be expressed as

$$W_1 = W_0\sqrt{1 + \left(\frac{g}{Z_R}\right)^2} \qquad (4\text{-}2)$$

and $$r_1 = g + \frac{Z_R^2}{g} \tag{4-3}$$

Where W_0 is the mode field radius of an SMF, g is the propagation distance from RP_{IN} (Plane 0) to RP_{OUT}, and Z_R is the Rayleigh range,

$$Z_R = \frac{\pi W_0^2 n}{\lambda} \tag{4-4}$$

After passing through the end face of the silica rod, the radius of the beam size W_2 and the curvature r_2 at Plane 2 becomes

$$W_2 = W_1 \tag{4-5}$$

and $$r_2 = \frac{r_1 f}{f - r_1} \tag{4-6}$$

where f is the focal length under paraxial approximation given by

$$f = \frac{\mathbf{R}}{1 - n} (\mathbf{R} < 0, f > 0) \tag{4-7}$$

Where **R** is the radius of the plano convex lens on the front end of the fiber. Thus, the focused beam waist W_i and working distance Z_i can be written as

$$W_i = \frac{W_2}{\sqrt{1 + \left[\frac{\pi W_2^2}{\lambda r_2}\right]^2}} \tag{4-8}$$

and

$$Z_i = \frac{-r_2}{\sqrt{1+\left[\frac{\lambda r_2}{\pi W_2^2}\right]^2}} \qquad (4\text{-}9)$$

respectively.

A hemispherical microlens at the front end is used as the collimating element. The length of the pure silica rod d is designed to control the beam waist Wi, which is defined as half-width at $1/e^2$ maximum intensity, and position Zi, which is defined as the distance from the beam waist position to the lens front end. The relationships of Wi and Zi as a function of propagation distance g = d + **R**, where **R** is the radius of the hemispherical lens under the paraxial approximation. The fiber collimator we designed is with g = 200 μm, the beam shape can be given by using the above formulas. The spot radius versus propagation distance was shown in Fig. 4-9.

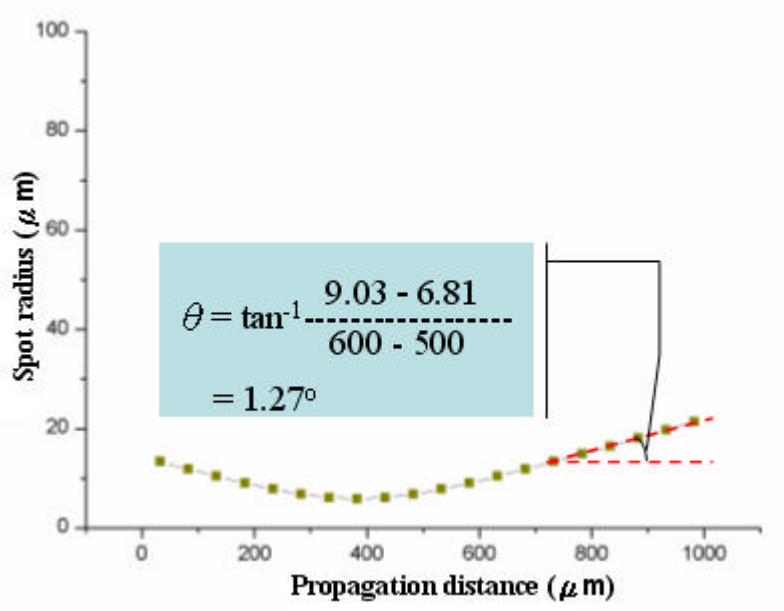

Fig. 4-9 Calculated spot size as a function of propagation distance

The minimum beam waist is located at 382.7 μm and has a nearly collimation beam (divergent angle ? = 1.27°) for a very long working distance (1mm). With the long working distance fiber collimator applied to the pickup, a loose tolerance system can be realized. Then, the fiberlens with g = 200 μm was put into the testing setup to verify the above mathematical description.

4.4.2 Measurement

The single mode fiberlens with g = 200 μm was placed in the measurement setup and light was guided into the fiber by the 2-axis (x-y) fiber coupler. The beam shape out of the fiber was determined by measuring the spot size at different positions away from the CCD. The result is shown in Fig. 4-10.

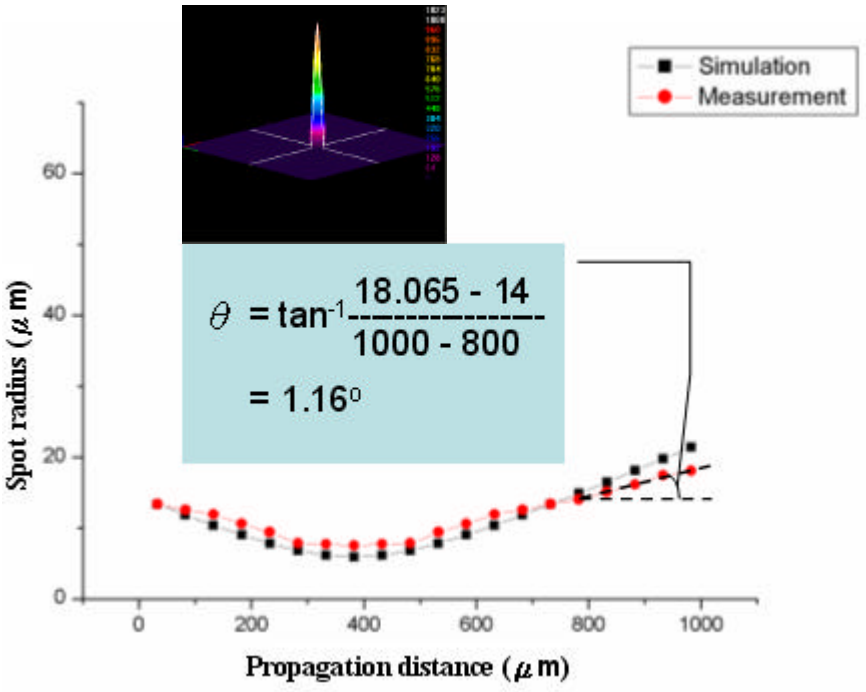

Fig. 4-10 Comparison of the simulation and the measured data

The distance between the fiber and the CCD was from 0 to 1000 μm, and the spot size was measured every 50 μm. A nearly collimated beam with divergent angle ? = 1.16° was realized. By applying the fiber collimator to the pickup system, the assembly tolerance can be increased and the light obstruction caused by the aperture can also be avoided.

4.5 Optical quality of the 45° mirror

In this experiment, two configurations were measured with the same setup. One is the pure fiberlens; the other one is the fiberlens/45° mirror combination, as shown in Fig. 4-11. The optical fiber was fixed in the V-groove by optical glue. Light was guided into the core from the other end of the fiber. The collimated beam out of the fiber was reflected by the microfabricated 45° mirror and the spot was measured and analyzed by the CCD.

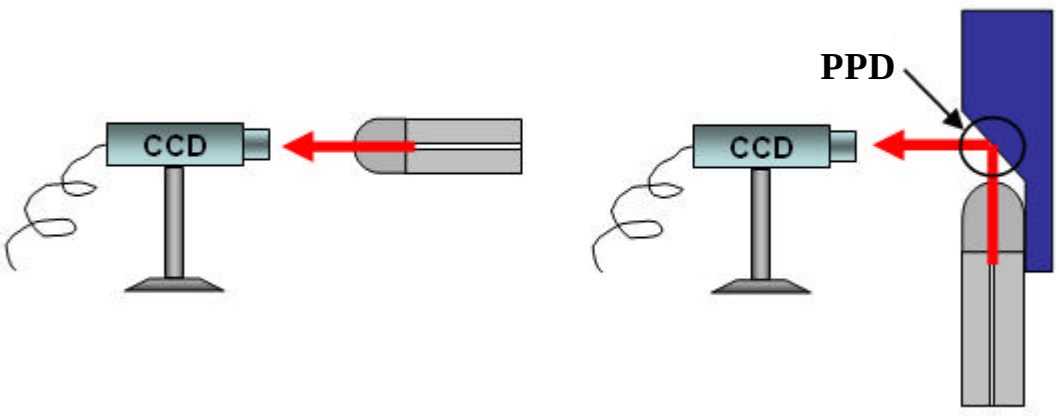

(a) (b)

Fig. 4-11 Schematic view of (a) the pure fiberlens and (b) the fiberlens/45° mirror combination

Due to the propagation path difference (PPD) caused by the fiberlens/45° mirror combination, the measured spot size would locate at the rear part of the beam out of the fiber. The spot radius versus propagation distance is shown in Fig. 4-12. The propagation distance is the distance between the CCD and the pure fiberlens (or the fiberlens/45° mirror chip). The initial measurement began at 8000 μm as a result of the geometrical limitation caused by the size of the fiberlens/45° mirror chip. The region formed by the measured curve and horizontal axis can be treated as upper part of the beam. Since the propagation path difference (PPD) caused by the combination of fiberlens/45° mirror, the spot radius curve would be shifted. The plot includes simulated data (square line) and measured data for pure fiberlens (circular line) and fiberlens/45° mirror chip (triangular line). From the result shown in Fig. 4-12, the curve of pure fiberlens fit closely to the simulation one. It means that a perfect hemispherical microlens can be fabricated on the end of the fiber by the splice machine. With the 45° mirror added, the propagation path difference (PPD) was induced because of the incontrollable gap between the fiber and the 45° mirror. Due to the propagation path difference, the curve of fiberlens/45° mirror was shifted from A' to A, and the shifted distance (about 330 μm) could be regarded as propagation path difference.

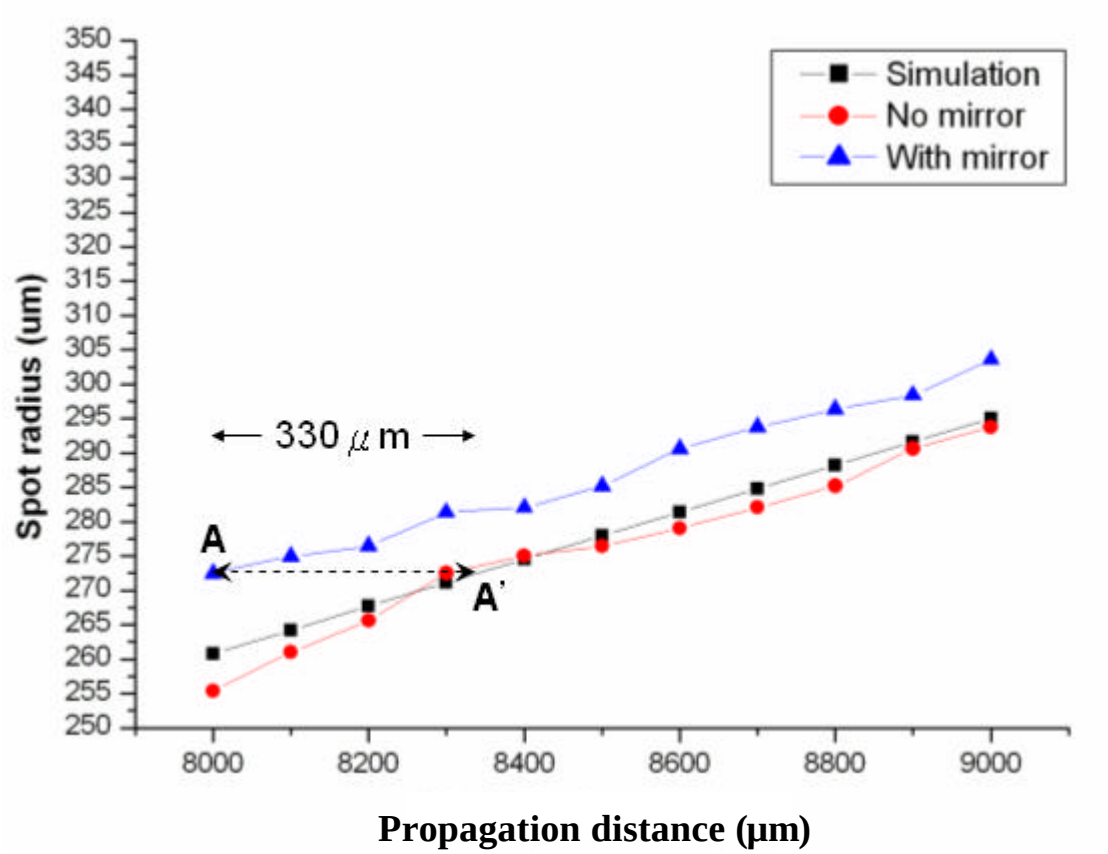

Fig. 4-12 The spot radius versus propagation distance graph of the cases of simulated, without mirror and with mirror added.

The reflectivity of the fabricated 45° mirror can be obtained by using the same measurement procedures. First, the pure fiberlens without mirror chip added was measured, and the corresponding intensity was revealed (square line). By measuring the combination of fiberlens/45° mirror chip, the related curve was shown closely to the pure fiberlens one . The diagram of curves is shown in Fig. 4-13. The reflectivity (about 93%) can be easily calculated by dividing any two intensity values at the same position and the propagation path difference (PPD) effect has been eliminated.

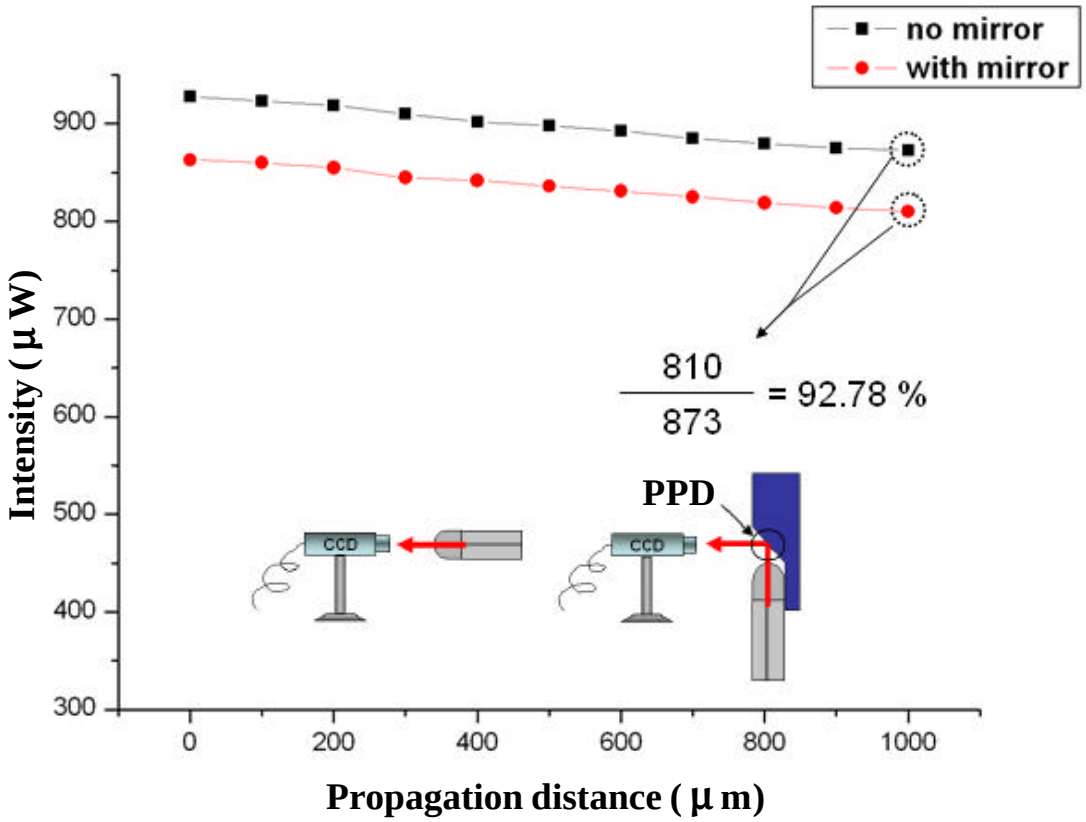

Fig. 4-13 The graph of intensity versus propagation distance for the cases of with mirror and without mirror added.

4.6 Summary

The effective NA (NA_{eff}), Seidel coefficient (W_{040}) and optical throughput efficiency of the pickup system has been evaluated and optimized. A fiber collimator applied to the pickup module can improve the system tolerance and make integration easily. Moreover, the reflectivity of 45° mirror and the beam shape out of the fiberlens/45° mirror combination were measured to prove the optical quality of the extreme smooth 45° mirror fabricated by wet anisotropic etching. The optimization of the geometry and fabrication process for enhancing system throughput, and further miniaturization of the overall size are undergoing for applications in ultra high density storage device.